FEDSM-ICNMM2010-30(, (

A CLOSED LOOP APPROACH TO SIMULATE THE UNSTEADY THREE-DIMENSIONAL FLOW IN AN AXIAL FLOW PUMP

Friedrich-Karl Benra, Hans Josef Dohmen
University of Duisburg-Essen
Institute of Energy and Environmental Engineering
Turbomachinery
P.O. Box 1629, Duisburg, 47048, Germany
E-mail: hans-josef.dohmen@uni-due.de

ABSTRACT

A new method is put forward to model the flow in a highly loaded axial flow pump. A directional loss model is utilized to model the function of a valve behind the pump stator vanes. A periodic boundary condition between the inlet and the outlet of the pump is applied to model a closed loop. Thus no flow specification in either the inlet or outlet of the pump is required; also it is not necessary to give the turbulence level. By this method no pressure level inside the flow domain is given by a boundary condition. To avoid numerical instability the pressure level has to be given at least at one grid point. A given constant pressure somewhere in the loop domain is physically invalid, especially at stall condition of the pump. This is avoided by introducing a reservoir with a constant pressure boundary condition that is nearly decoupled from the pressure field inside the main pump loop by a huge flow resistance. Consequently this method can avoid specifying non-physical stationary boundary conditions at the inlet and the outlet for transient simulations.

The new model can predict the mass flow fluctuations in the pump. These fluctuations are not very strong at stable operating conditions but increase in part load or stalled flow conditions. The transient numerical results obtained by the new approach are compared with those obtained by the conventional simulation with stationary boundary conditions (constant total pressure at the inlet and fixed mass flow at the outlet) and also with results of experimental investigations performed by Kosyna and Stark.

The different flow structures inside the blade passages of the pump are described and compared in detail for part load, overload and design point as well as for stalled flow conditions.

KEYWORDS: Axial-flow pump, unsteady Navier-Stokes equations, pump characteristic, directional loss model, vortex breakdown

INTRODUCTION

The head characteristic of highly loaded axial flow turbomachines is usually unstable. The unstable part of the head characteristic is normally reached by reducing the flow rate below 60% to 70% of the design mass flow rate. The drop in pump head is one visible change for the pump operator. Besides this, a strong increase of mechanical vibrations and NPSH3 values limit the operating range more than the drop of the head itself.

When it reaches the stall region of the pump the flow structure inside the machine changes dramatically. This is mainly induced by the part load vortices that appear in the hub region at the blade trailing edge and in the tip region at the blade leading edge. The strong time-variant behavior of these vortices leads also to very time-variant behavior of all flow parameters inside the pump and the attached pipes.

In previous studies the pump with a specific speed of $n_q = 150$ investigated here was tested with experimental methods [1,2,3,4] and also numerical investigations [5,6,7,8] were performed. All experimental results used in this paper were

obtained at the University of Braunschweig under the guidance of Prof. Kosyna and Prof. Stark. The experimental investigations show the flow structure in stable operation when reaching stall as well as in fully developed stall. Some of the experimental investigations deal with methods to stabilize the head characteristic at part load conditions by the application of casing treatment or by modification of the inlet nozzle geometry. The effects of the changes in geometry are also reproduced by numerical investigations.

All these numerical studies are performed with an ordinary numerical model that contains an inlet and outlet boundary of the computational domain. At these boundaries constant values (e.g. static pressure, mass flow, turbulence level) are given as boundary conditions for the numerical procedure. Particularly at stall operating conditions these values are highly time-dependent. Given that the experimental investigations are done in a usual test stand with a closed loop of the water the physically unrealistic assumption of constant boundary conditions could have an influence on the numerical results in these operating points.

NOMENCLATURE

| g	m/s^2	gravitational acceleration
H	m	pump head
n	s^{-1}	rotational speed
Q	m^3/s	volume flow rate
n$_q$	-	specific speed $(333\frac{n\sqrt{Q}}{(gH)^{3/4}})$

subscripts

Bep	-	Best efficiency point

NUMERICAL MODEL

For the previous investigations [6-8] an ordinary set-up of the numerical model was used. In these configurations the computational domain was assembled from a non-rotating inlet part and a rotating part containing the impeller blade followed by an additional stationary part containing the stator vanes. The connection of the different part domains was made by an ordinary sliding rotor stator interface for the transient simulations. For all simulations the same overall topology of the part domains and, when possible, the same meshes were used. To simulate the casing with grooves [7] the inlet part domain ends in the tip region only 2 mm in front of the impeller leading edge. In a normal set-up without the geometrical restrictions of the grooves this interface should be located in a larger distance in front of the impeller. This has to be done because at this interface the governing equations are not solved consistently and so a disturbance of the solution by the interface will appear.

Figure 1 looks more closely at the computed flow field in the tip region of the leading edge for a configuration without casing treatment in front of the impeller. The rotor blade colored with the static pressure is presented. The streamlines starting in the tip gap, integrated only in forward direction and
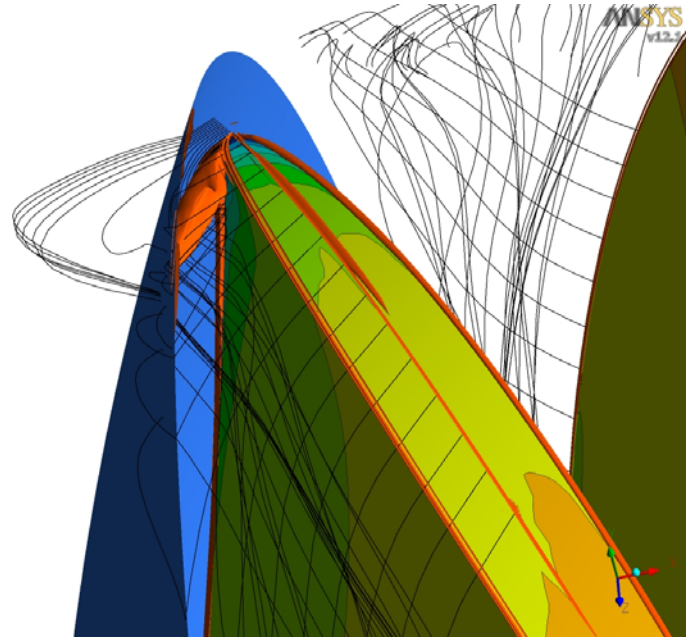
Figure 1: Influence of sliding rotor stator interface on numerical results Q/Q$_{BEP}$= 0.76.

forming the tip clearance vortex, are added in black. Also the surface of the sliding rotor stator interface is shown in blue in front of the impeller blade. Between this surface and the blade in the part where the tip clearance vortex is located a vortex core region with constant swirling strength is shown. All vortex core regions shown in this paper are isosurfaces of constant swirling strength. It seems that the rotor stator interface is an insuperable fence for the vortex core region. This effect can also be found in other variables but for best visualization this example was chosen here. It is clear that this gives a strong disturbance to the prediction of the flow field in the tip region and especially to the prediction of the tip clearance vortex.

For this reason the mesh of the rotating blade domain was modified so the sliding rotor stator interface was approximately 1.5 pump diameters in front of the impeller blade to prevent disturbance to the tip leakage flow by the interface, as shown in figure 2. Unfortunately the hub of the pump ends very near to the front of the impeller. The interface is now located in a region without a hub wall so one grid node is placed on the axis of rotation. This leads to numerically unstable behavior in the used numerical code. To avoid this, a very small hub with a diameter of 1 mm and a length of 6 mm was introduced in the interface region (see lower right picture in figure2). The structure of the mesh also has to be changed from the usual y-structure used in the part without hub to a normal h-structure used in geometries with hub. This gives a complicated mesh structure in the part near the rotation axis with an interpolation interface in front and one behind the sliding rotor stator interface (see upper left picture in figure 2). The radial outer part of the mesh is unchanged. The boundary condition at this hub wall is given as a free slip wall. No disturbance of the pressure or velocity field by this additional hub wall was found
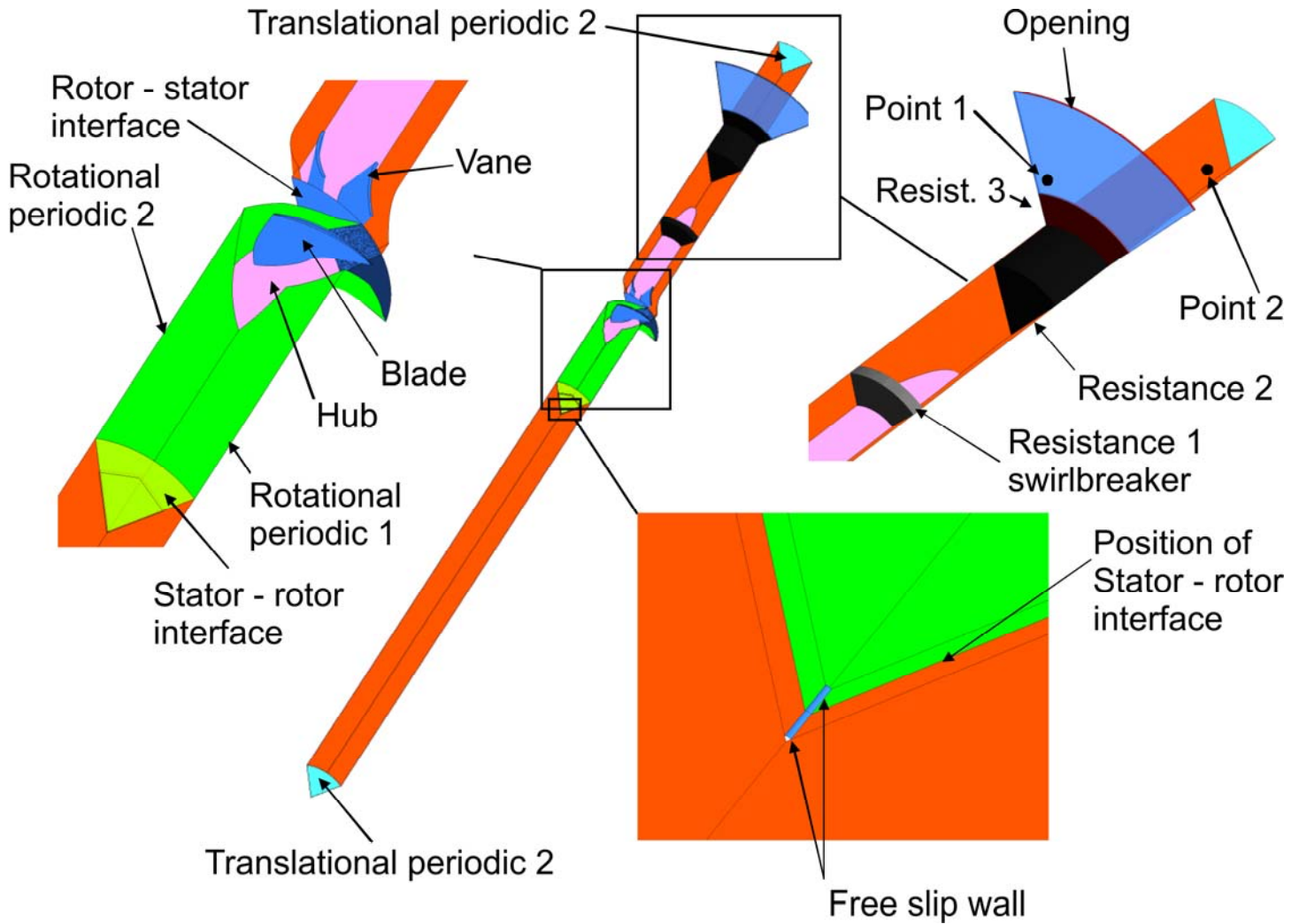
Figure 2: Numerical model.

in the computed results. In the experiments the inflow passage with a constant diameter of 0.35 m had a length of 4 m. The length of the inflow passage in the numerical model was 3.5 m. The length of the outlet part behind the stator vanes was 1.5 m.

The simplification used in earlier investigations to increase the number of stator vanes from eleven in the pump to twelve in the computation to get a common number with the six impeller blades is also used here. This reduces the numerical effort of the simulations by a factor of six for these first calculations. In further calculations a complete pump (six impeller blades, eleven stator vanes) without the assumption of circumferential periodic flow conditions in each blade passage should be investigated. The geometry behind the stator vanes is enlarged and the hub of the pump ends a certain distance behind the vanes (see upper right picture in figure 2). This is done to get a surface at the end of this part domain (Trans. periodic 2) that is congruent to the surface at the beginning of the inlet domain (Trans. periodic 1). In the numerical set-up these two surfaces are defined as translational periodic. This means the flow leaving at Trans. periodic 2 enters Trans.

periodic 1 directly in front of the impeller. The ordinary boundary definitions of the pump walls with a no-slip condition in the appropriate frame of reference and the rotational periodicity in the circumferential direction must be defined. But no inlet and outlet boundary condition is necessary.

With a set-up like that, however, the pressure level in the computational domain is not given. To avoid numerical instability the used code will fix the pressure at one grid node to a constant value of zero bar. (The absolute value of the pressure is not of interest in a pressure correction method for incompressible fluid without consideration of cavitation because in the governing equations only gradients of the pressure are present.) To avoid this constant pressure at a random position in the computational domain a slit is introduced in the casing wall behind the pump followed by a radial diffuser (see upper right picture in figure 2); the outer surface of this diffuser is defined with a constant pressure boundary condition that allows the flow to enter or leave the computational domain. To maintain stability of the numerical code and to be able to change the operating point some parts of

the mesh are defined as a porous medium that has a specified resistance to the flow. The regions are marked in the upper right picture of figure 2 in dark color. The first resistance is for numerical stability only. In part load conditions the flow leaves the vanes with a strong circumferential velocity component and in the area in which the hub radius becomes zero the circumferential velocity increases to unrealistic values by conserving the angular momentum ($c_u r = const.$). In resistance 1 a small resistance is given for the axial velocity component but a huge multiplier for the circumferential and radial component is used. This resistance acts like a flow straightener used in experiments to eliminate the circumferential velocity component in the flow field to get a swirl-free flow field in front of the impeller. The resistance 2 located downstream of the pump in the connecting pipe is used to model a valve. If the value of the resistance is increased, the valve is closed, and vice versa. The third resistance located in the inner part of the radial diffuser was given with a very huge value to decouple the flow path from the ambient given by the constant pressure boundary condition. This allows the pressure in the flow domain to change in time, almost unaffected by the constant boundary condition. This is analogous to a reservoir filled with a gas used in a closed loop test stand to fix the pressure level inside.

In this paper all operation points are at a rotational speed of the pump of n = 1000 min^{-1} given as a property of the impeller domain. The simulations are carried out on a block-structured hexahedral mesh that contains 1.97 million grid points. The minimum geometric angle in the mesh elements is higher than 20 degrees. The Y^+ values for all simulations are lower than 40 in all domains. The turbulence was modeled by a k-ω turbulence model using a SST near wall formulation. The spatial discretisation was of second-order accuracy and the time discretisation was second-order backward. The convergence criterion for the transient simulation was a maximum RMS value lower than 1×10^{-3} in each time step for all residuals in all part domains. The time step for the calculations (unless indicated otherwise) has been chosen to 5×10^{-4} s to encounter the periodic positions for the rotor and the stator during the revolution of the impeller. This gave an impeller rotation of 3deg for each time step.

The trend of the static pressure at the observation point 1 in the radial diffuser and point 2 in the pipe behind the resistance 2 (in front of the impeller, see upper right picture in figure 2) is displayed in figure 3. In the lower part the static pressure at point 1 normalized with the constant outlet pressure is shown for the last ten impeller revolutions for Q/Q$_{BEP}$=0.66 at stall conditions. Additionally the average of the pressure is shown as a red line with a value of one so the average equals the boundary condition. In the upper part of this figure the pressure at point 1 behind the huge decoupling resistance is compared with the pressure in the pipe behind 'valve' resistance 2. Because the slit of the diffuser is located nearly at the end inside resistance 2 some losses occur in axial direction in the main flow path between the slit position and the position
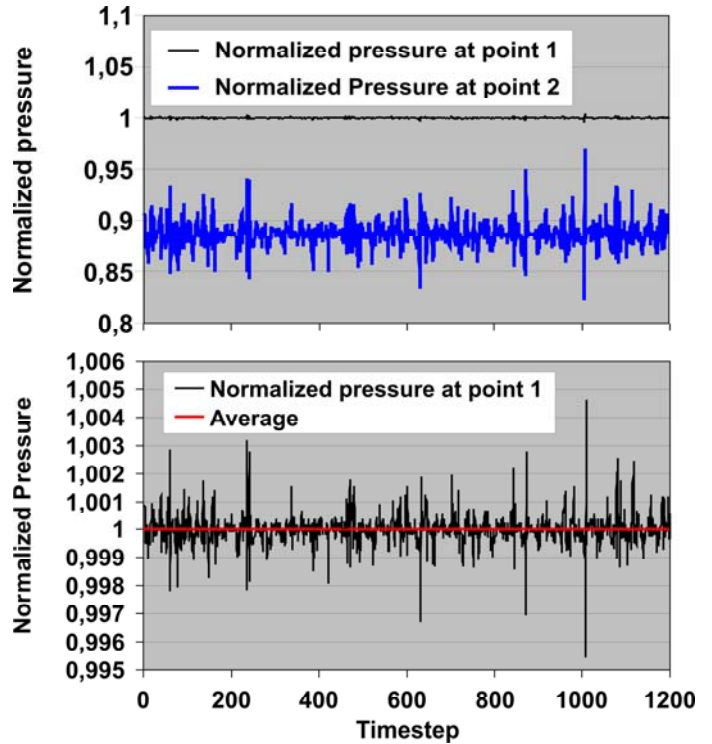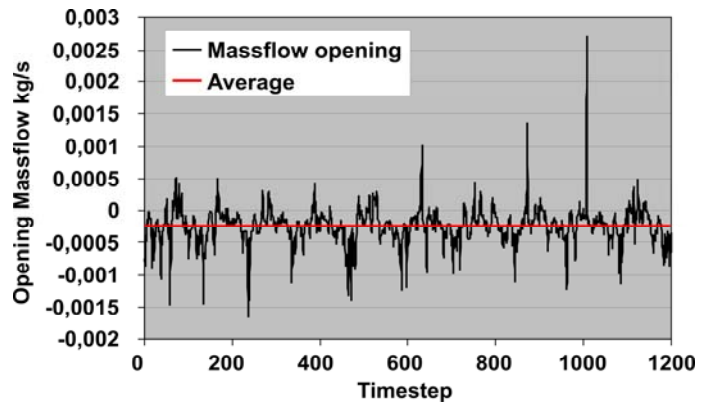

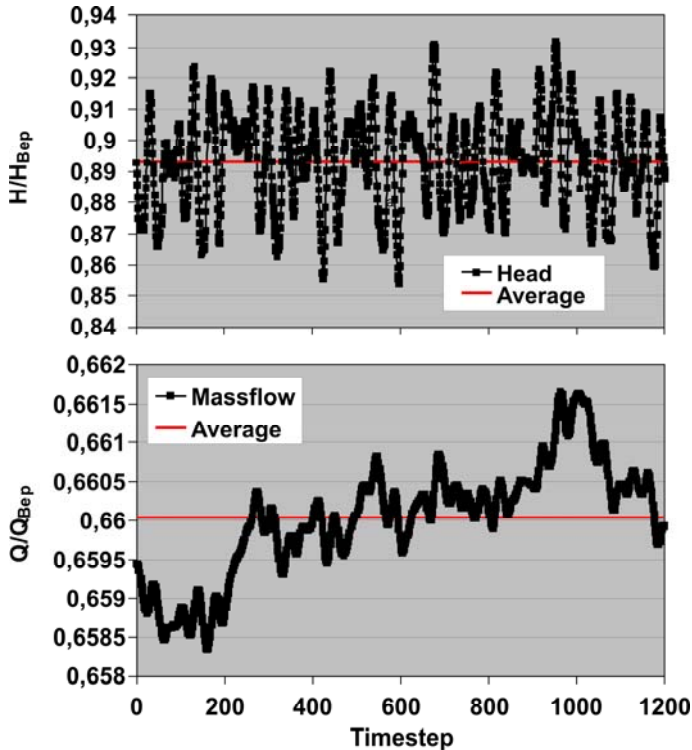**Figure 3: Pressure fluctuations during calculation Q/Q$_{Bep}$=0.66.**

of point 2. This gives the lower value of the pressure at point 2. In the different scales the decoupling of the pressure in the main flow path with a variability of 5% compared with the pressure at point 1 with a variability of 0.2% can be observed.

In figure 4 for the same impeller revolutions the mass flow at the opening position is shown as trend and also as average. It shows the change of the flow directions during the pump operation with almost time-periodic behavior. The physically unrealistic average (negative means outflow) unequal to zero can represent an accuracy problem in the numerical set-up and has to be investigated further.

The development of the head and the mass flow during the last ten impeller revolutions is given in figure 5. The average


Figure 4: Mass flow at opening Q/Q$_{Bep}$=0.66.

Figure 5: Development of mass flow and head during calculation Q/Q$_{Bep}$=0.66.

that is also shown is used to mark a point (x) in the head characteristic of the pump given in figure 6. The fluctuations of head and mass flow are high, especially at this operating point. The difference between the lowest and highest value of the head is approx. 9% of the average for this operating point. The trend of the mass flow also shows a random behavior for the ten impeller revolutions displayed. For operating points in the stable flow regime the comparable curves are much smoother. That means that for such operation points the assumption of constant boundary conditions should have no influence on the results.

RESULTS

Figure 6 shows the dimensionless head versus the dimensionless mass flow rate. Reducing the mass flow rate starting at overload conditions leads to an increase of the head. With a stronger reduction of the mass flow the characteristic stays stable. In the operating point at Q/Q$_{BEP}$ = 0.73 the characteristic becomes unstable. This unstable operating range ends with the first stable operating point at deep stall with a mass flow rate of Q/Q$_{BEP}$ = 0.65. The loss of head in this unstable range is nearly 30% of the design head of this pump. To compare the measured results with the results obtained numerical four operating points are computed with the new numerical model. The overload (1) and the design (2) point show a good agreement compared with the measured values obtained by Golz [1]. In terms of reaching the unstable operating conditions (3) the differences between measurement
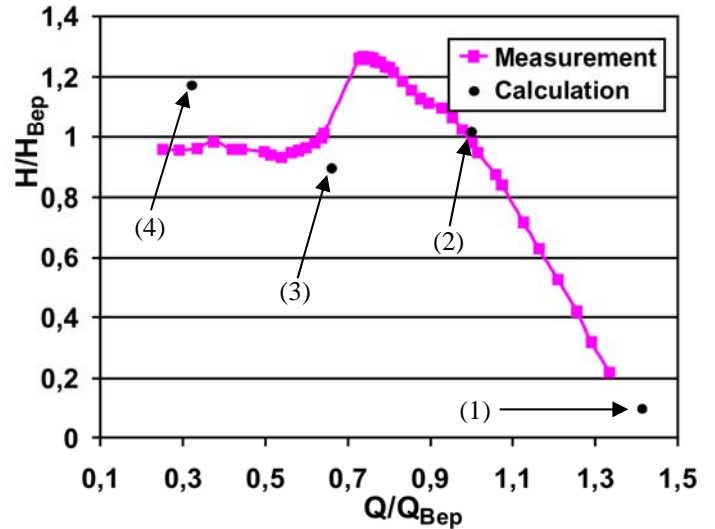

Figure 6: Pump head characteristic measured by Golz [1].

and calculation are more significant. In the deep stall region (4) the agreement is of poor quality. Comparing the computed results with the results obtained in previous calculations [5, 7] we see that the agreement of the new part load results are of poorer quality. An explanation for the differences in the unstable operating range is not available at the moment. The points representing the calculated results are always the average of the head and the mass flow of the last ten computed impeller revolutions in which no significant change in these overall quantities is observed. Therefore a very high computational effort for each operation point is necessary because the resistance value of flow resistance 3 must be adjusted over a lot of impeller revolutions to reach the required operating conditions. Simulation of the last ten revolutions for averaging requires less effort. Further investigation of the reasons for these differences at part load is essential.

FLOW STRUCTURE AT SHROUD

In the next figures the flow structure in the shroud wall boundary layer is shown. In the upper part of figure 7 the structure of the flow field in the wall boundary layer is visualized by oil flow pictures [2] for the design point of the pump. The flow structure with the separation in three regions is described in detail in [2]. The three regions are as follows:, at the left, the incoming flow in axial direction parallel to the pump axis; in the middle part, above the impeller blades, the flow that is mainly in the opposite direction; and the region behind the trailing edges of the impeller blades where the flow is attached to the wall and leaves in positive direction. The lower part of figure 7 provides the numerical results obtained. Besides the wall streamlines in black are shown lines of constant static pressure at the shroud surface (blue), the vortex core region of the tip clearance vortex (green) and the tip surface of the impeller blade (red). The flow structure given by the wall streamlines does not look as regular as that in the oil flow picture. This is a result of the fact that the oil flow picture

Vortex core region
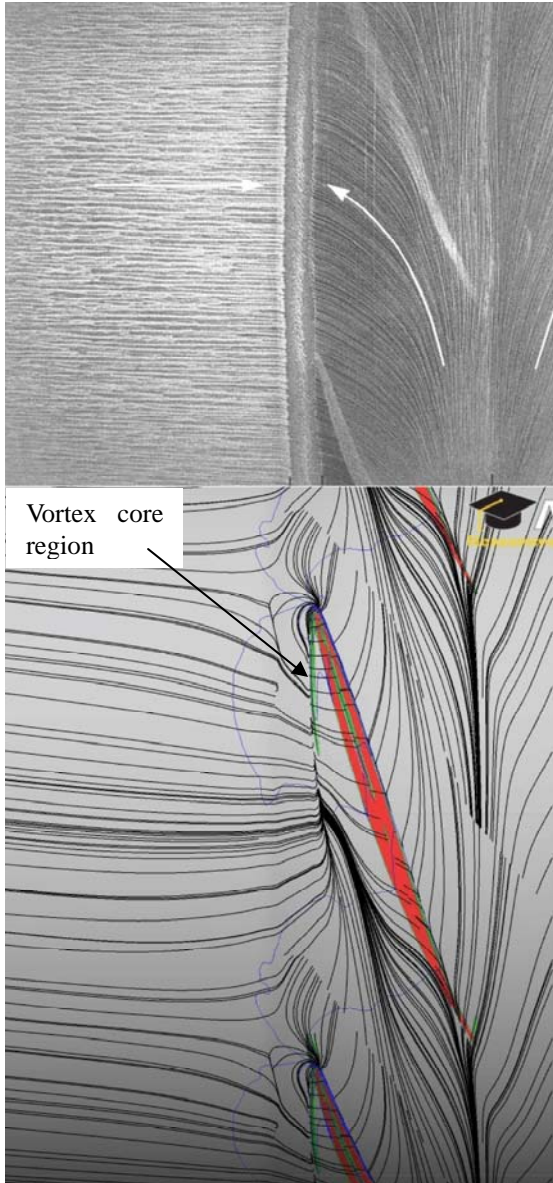
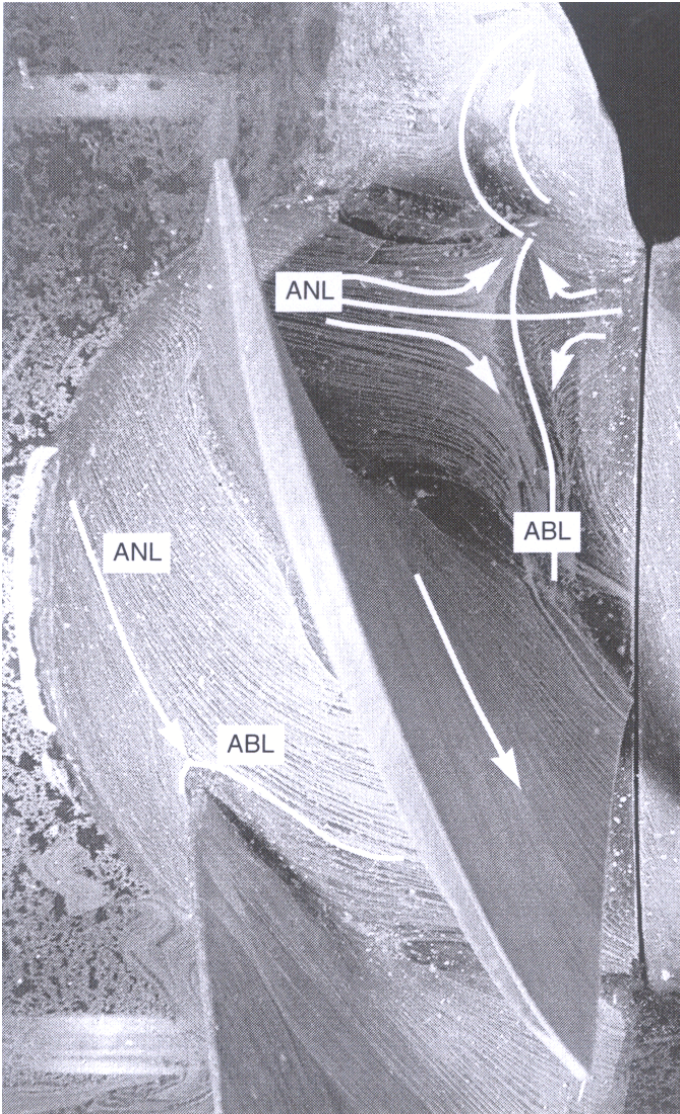**Figure 7: Rotor shroud wall streamlines at Q/Q_Bep=0.96.**

is a time average of the flow structure impressed into the paint during several impeller revolutions. The numerical results represent a snapshot of the flow structure at a certain time. Additionally the wall streamlines are broken by the post-processing procedure at the interface in the numerical mesh located in the tip gap almost above the mean line of the blade profile. Observing the numerical results in detail we see clearly that the separation line found in the oil flow picture at the impeller blade leading edge is a result of the tip clearance vortex induced by the tip clearance flow. The computed positions of the separation and attachment lines for this operating point compared with the oil flow picture are nearly identical.

In figure 8 the situation for the first stable operating point under stall conditions is displayed in the same way. As
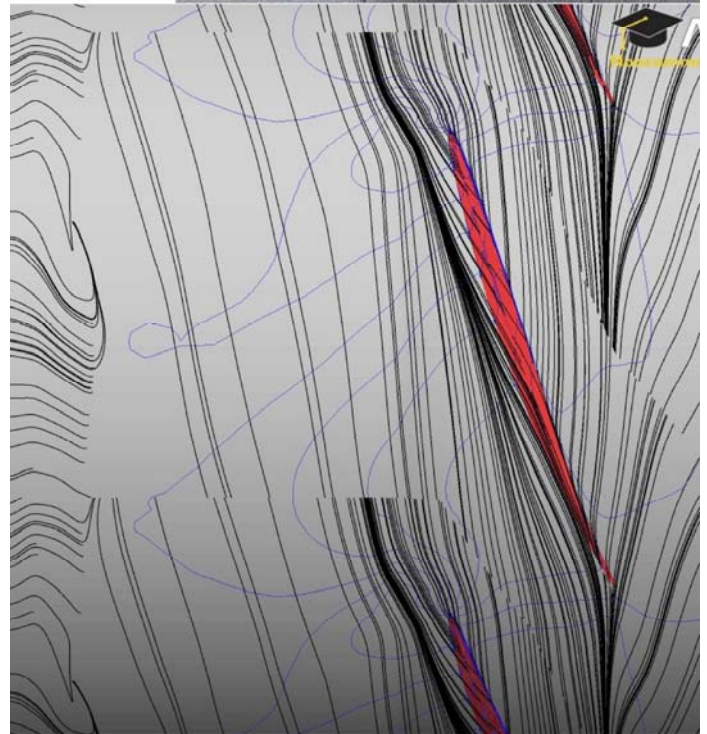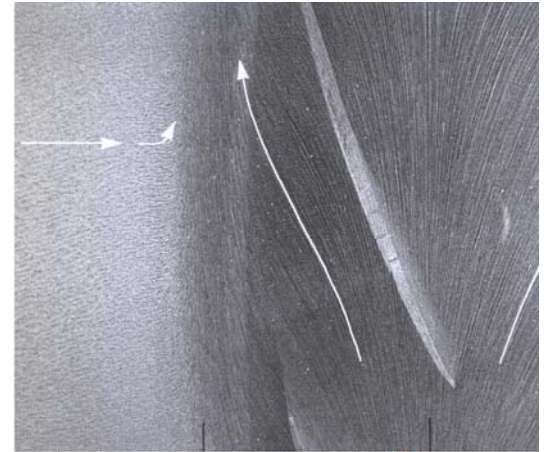
Figure 8: Rotor shroud wall streamlines at Q/Q_Bep=0.66.

observed by Golz [2], the separation line at the blade leading edge is moved to a position more axial upstream and the attachment line is nearly independent of the mass flow rate. In the computation the position of the separation line moves to a position located much more upstream than that found in the experiment. The vortex core region is not included in this figure because for this operating point no tip clearance vortex is present, as can seen by the streamlines starting in the tip gap and moving directly in upstream direction. Also, here the streamlines are broken at the interface in the tip gap. The big difference between measurement and computation in the axial velocity profile for this operating point in front of the impeller is also shown in [6,7] for a computation with the ordinary time constant boundary conditions. The same differences in the axial velocity profiles found there are found in the calculation

Figure 9: Rotor hub wall streamlines at Q/Q_{Bep}=0.96.

presented here. The difference now shown in the flow field which is already starting inside the shroud wall boundary layer could give an important clue to the reason for the difference: it could be the representation of the walls as smooth walls in the numerical model compared with the real pump wall that has a technical roughness. An investigation into the influence of the representation of the wall roughness in the numerical model on the numerical results could suggest additional ways to solve this problem.

FLOW STRUCTURE AT HUB

In the next figures the flow structure inside the blade passage is visualized and the numerical results are verified with oil flow pictures obtained experimentally by Golz [1]. In the oil flow picture in figure 9 the flow structure at the hub and the blades of the impeller is displayed. To make the structure of the flow field at the hub clearer Golz [1] added white lines to indicate the flow direction, and to mark separation (ABL) and
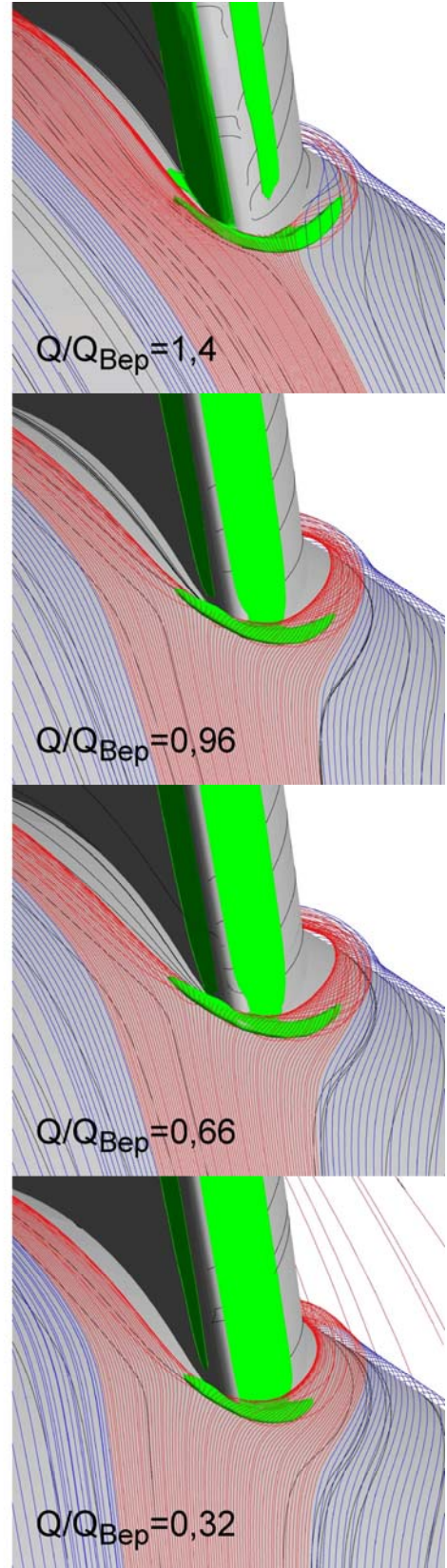
Figure 10: Streamlines in hub boundary layer in front of rotor blade at different operating points.

attachment lines (ANL). In her discussion of the flow field near the hub she indicates a saddle point in front of each blade. Starting at this point she detects separation lines at the suction and the pressure side of the blade. The suction side separation line follows the blade contour. The pressure side separation line crosses the blade passage from the pressure side to the suction side driven by the pressure gradient.

Figure 10 gives a detailed view of the computed flow field near the blade leading edge at the hub for different operating points. The wall streamlines in black show comparable structures to the structures visualized by the oil flow pictures of [1] in figure 9. The starting position to visualize the flow structure near the impeller hub based on the numerical results is a line 0.5 mm above the hub wall axial in front of the blade. At this line additional streamlines are created. To make the origin of the flow clearer in the following observations the streamlines directly in front of the blade are colored red and the ones in the blade passage are blue. The changed mass flow rates in the different operating points lead to different directions of the relative flow vector. In all operating points the hub boundary layer separates in front of the blade leading edge forming a horseshoe vortex. This is not only indicated by the streamlines as the included vortex core region colored green also clearly shows the presence of this vortex. In the operating points with high mass flow rate the suction side part of the vortex is much stronger than the part at the pressure side. Reduction of the mass flow means that the suction side part of the vortex is diluted.

FLOW STRUCTURE INSIDE BLADE PASSAGE

To make the structure and the changes of the flow field with operation point clearer figure 11 has been generated. In this figure the wall streamlines at the suction side of the blades and the hub colored black are shown, together with the streamlines in the hub boundary layer already described in the discussion of figure 10. To validate the numerical results the available oil flow pictures for the same operating points obtained by Golz [1] are shown at the left side. As already seen in figure 10, most of the red streamlines for Q/Q_{Bep}=1.4 are directed to the pressure side of the blade by the changed relative flow direction in front of the impeller. Near the trailing edge in the corner between suction side and hub the flow is separated and a vortex nearly perpendicular to the main flow direction is generated in the blade passage at the hub. The generation of this vortex is favored by the hub contour. This corner stall was identified by Golz [1]. The part of the boundary layer flow that was marked by red streamlines in front of the blade leaves the blade passage in the hub blade corner at the pressure side of the blade. Then it moves around the trailing edge and becomes part of the described vortex at the hub.

Reducing the flow rate to Q/Q_{Bep}=0.96 changes the direction of the flow in front of the blade. Consequently, more of the red streamlines are directed to the blade suction side. These streamlines follow the shape of the suction side. At the

trailing edge most of them are not included in the hub vortex but are guided along the last part of the suction side blade contour in radial outward direction. The vortex at the rotor hub is now more regular compared with overload conditions.

The situation at the hub for the first stable operation point with stall conditions Q/Q_{Bep}=0.66 has not changed very much compared with design conditions. The separation region at the trailing edge of the suction side has moved closer to the trailing edge. This cannot be found in the oil flow picture. Slightly more of the red streamlines are following the suction side contour, but fewer of them are directed radially outward. The others are included in the hub vortex. The main changes compared with Q/Q_{Bep}=0.96 are in the tip region caused by the change of the tip leakage flow structure, compared earlier in figures 7 and 8.

The flow field changes more dramatically by reducing the mass flow rate to deep stall conditions Q/Q_{Bep}=0.32 with about 30% of the design mass flow rate. The relative inlet flow angle is again changed and more of the red streamlines are following the suction side contour of the blade. The position of the corner stall compared with the overload point is almost unchanged. The part of the flow that is directed radially outward, however, now reaches the shroud and forms an additional vortex structure on the way from hub to shroud. On the blade suction side itself the structure of a cross-passage vortex is visible. This structure at the blade suction side is also found in the same position in the oil flow picture. As regards the flow situation at the position of the hub suction side corner near the blade trailing edge where the corner stall occurs a detailed view is displayed in figure 12 for the four investigated operating points.

In the representation of Q/Q_{Bep}=1.4 no structure of the flow at the suction side is visible. The only structure that is remarkable is formed by the red streamlines coming around the blade leading edge.

For Q/Q_{Bep}=0.96 the basis of the hub vortex can be seen in the corner. To make this clearer, the vortex core region in green that was used in figure 10 is additionally included in these figures.

For Q/Q_{Bep}=0.66 this core region diminishes almost completely. The core region found at this position for Q/Q_{Bep}=0.66 is not part of the hub vortex. It is now the basis of the vortex structure that is formed from hub to shroud at the leading edge part of the blade suction side. This core region is surrounded mainly by red streamlines coming from the suction side part of the horseshoe vortex in front of the blade.

To illustrate the changes in the structure of the flow field better, figure 13 is the view towards the blade pressure side for all investigated operation points. As in figure 11, the relevant oil flow figures from Golz [1] are added at the left side. To get a better impression of the flow structure at the pressure side another set of streamlines is introduced. These green streamlines start at the pressure side of the blade at the leading edge 3.5 mm above the hub wall.

Copyright © 2010 by ASME

For Q/Q$_{Bep}$=1.4 the different behavior of the boundary layer flow in red and blue, mostly turned around the blade trailing edge, to be introduced into the separation at the end of the suction side, and the flow above the boundary layer in green following the direction given from the blade passage is remarkable.

For Q/Q$_{Bep}$=0.96 the situation changes. The red streamlines enter directly into the now increased hub vortex established across the blade passage. In this operating point the hub vortex has already a diameter that influences the direction of the green main flow. The hub vortex of one blade is moved in flow direction on the way from suction to pressure side so it passes
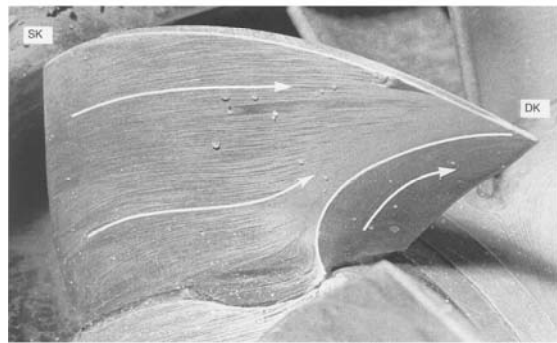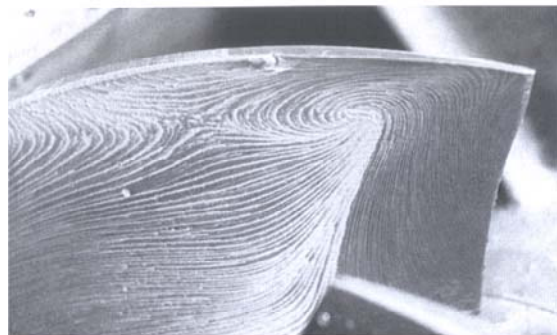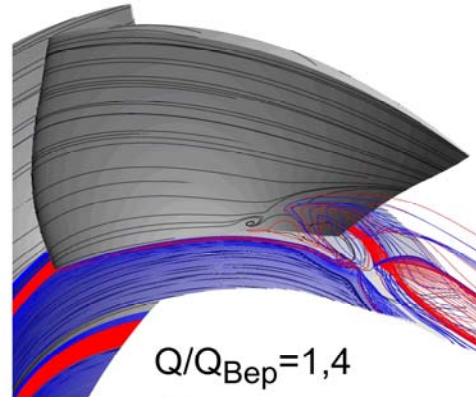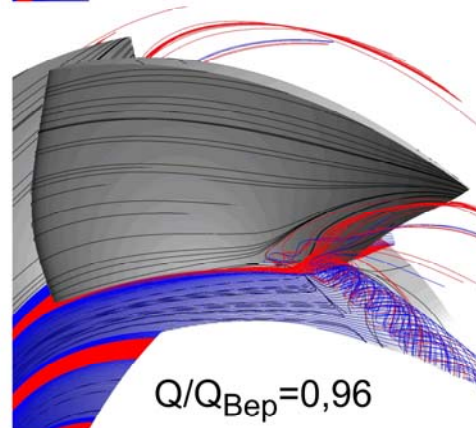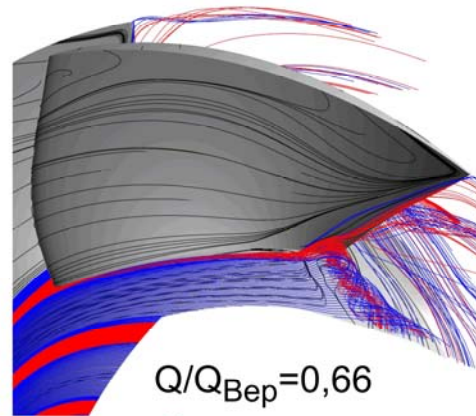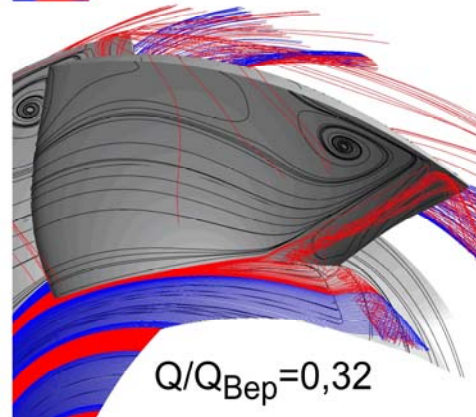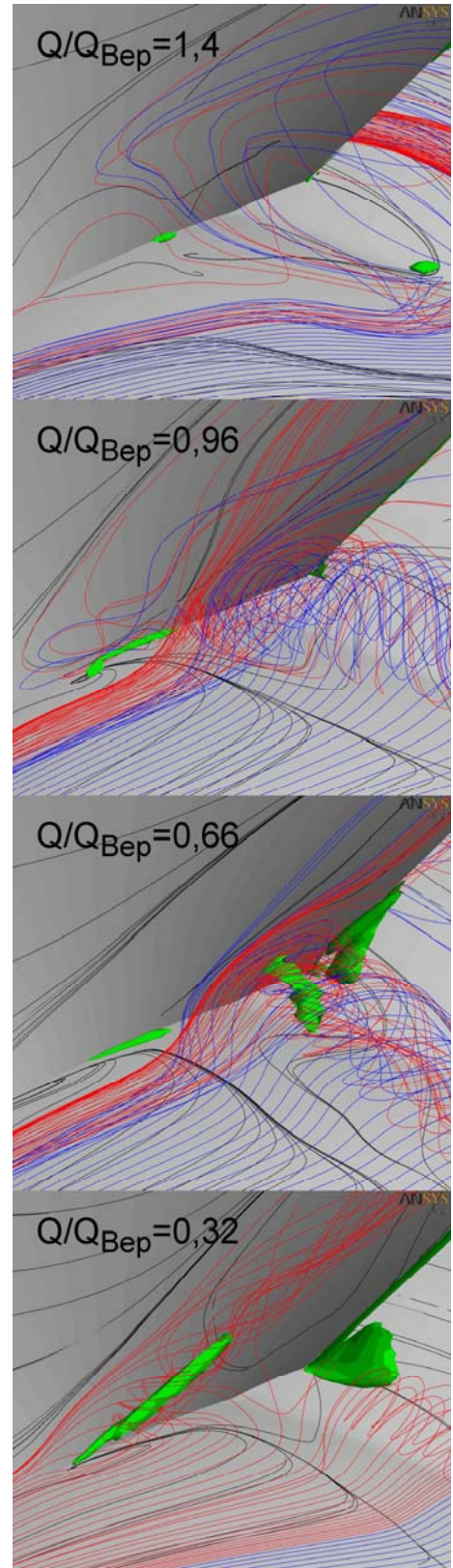

Figure 11: Wall streamlines at blade suction side and streamlines in hub boundary layer starting in front of impeller blade.

the next blade behind the trailing edge. In contrast to the nearly unchanged situation found at the suction side for Q/Q_{Bep}=0.66 the situation at the pressure side changes significantly. The hub vortex is further increased in size and is lifted from the hub wall, coming to the pressure side of the next blade. In addition it is shifted in upstream direction so it hits the trailing edge of the next blade at the pressure side. This structure agrees with the structures found experimentally by the oil flow picture from Golz [1]. The green streamlines of the main flow are moved upward in radial direction reaching nearly one-third of the blade height. The green streamlines starting very close to the pressure side blade wall 3.5 mm away from the hub wall at the leading edge are moved upward to two-thirds of the blade height.

At Q/Q_{Bep}=0.32 the hub vortex starts directly at its origin to move radially outward, as seen in the left part of the lowest part of figure 13. The diameter is not increased further, but it reaches the shroud when it passes the trailing edge of the next blade, so a huge part of the passage area is blocked by this vortex. This is mainly the suction side part of the blade passage at the shroud. Some of the fluid which was moved radially upward in the small vortex at the suction side passes the tip clearance and is transported in upstream direction in the shroud boundary layer as seen by the red streamlines.

Now we will reconsider Q/Q_{Bep}=0.32 in figure 11. In this view the hub vortex blocking the blade passage behind the trailing edge is rotating in clockwise direction. The main flow that enters the blade passage in the mid-section at the suction side hits this vortex and is deflected in a radial outward direction and at the shroud wall in a direction reverse to the main flow direction and additionally by the tip leakage in a direction to the next pressure side. The main flow at higher radial sections gathers the observed fluid. This collision changes the direction of the observed fluid again to a radial inward direction. The result is a large vortex structure rotating in counter-clockwise direction that is already seen in the oil flow picture and the computation shown in figure 11.

This mechanism at Q/Q_{Bep}=0.32 is illustrated in figure. 14. Here streamlines are generated at constant radii in front of the impeller blades. To get a clear view of the region of interest only a downstream integration of the streamlines is performed. In the upper right part the streamlines are generated at 71% blade height. These streamlines are colored with the static pressure (blue low pressure, red high pressure). To get a better impression of the situation at the suction side, only in this figure the red streamlines starting in front of the blade leading edge in the hub boundary layer explained in figure 10 are additionally included. It is clear already at this radius that the main flow at the suction side is deflected radially outward and also turned towards the pressure side. In the last third of the suction side the flow is separated from the blade and boundary layer material from the hub is transported to the shroud, as can be seen by the red streamlines.

Figure 12: Wall streamlines at blade suction side and streamlines in hub boundary layer starting in front of impeller blade.
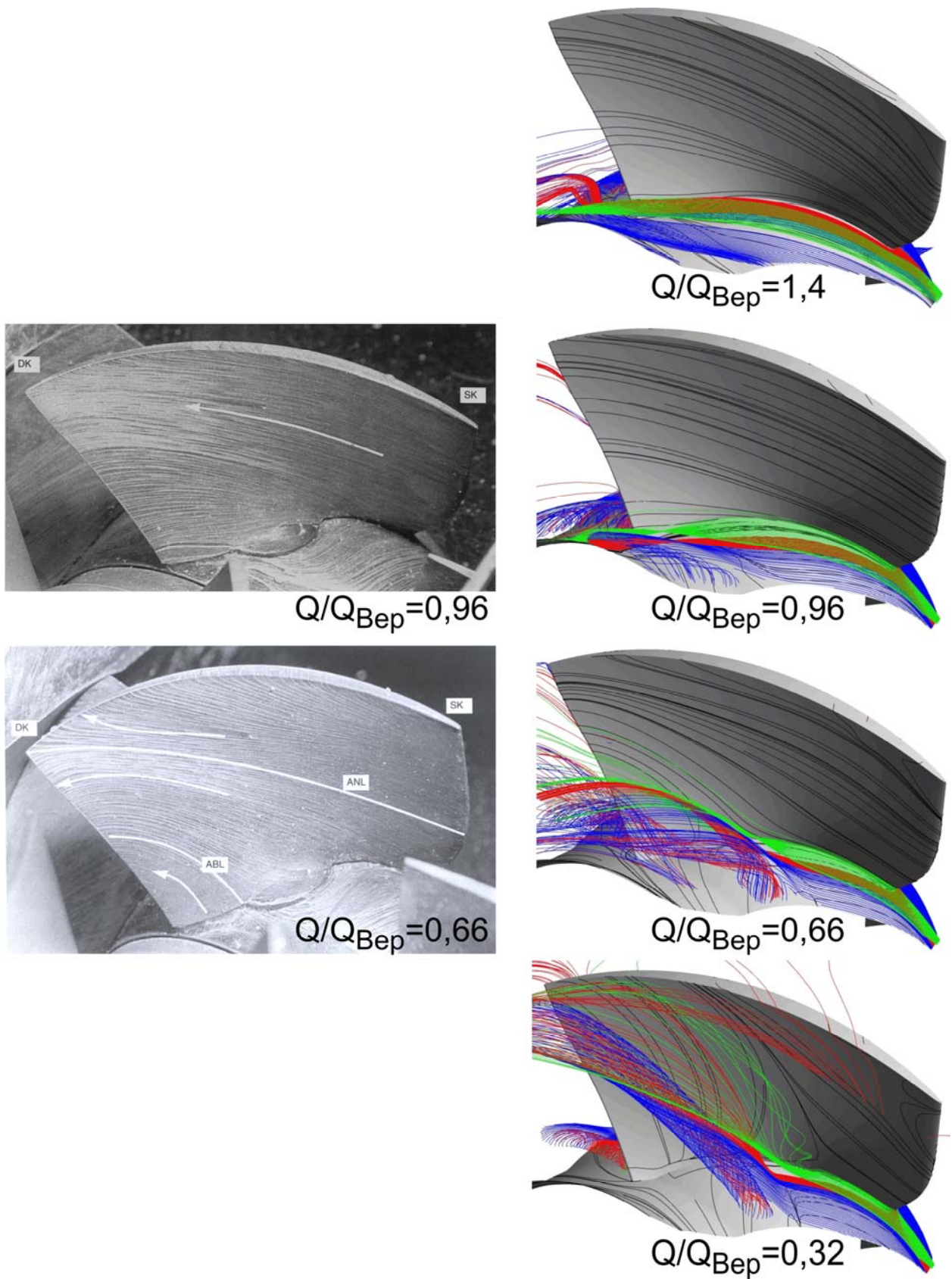
Figure 13: Wall streamlines at blade pressure side and streamlines in hub boundary layer starting in front of impeller blade.

When the streamlines start more radially outward at 81% blade height the cross-passage vortex in the whole blade passage becomes visible. Comparing this flow visualization of the numerical results with the photograph of the cavitating vortex core taken by Golz [1] shows a good agreement of the position of the computed vortex core compared with the reality.

The next streamlines starting at 95% blade height are shown in the lower part of figure 14. It is clear that the complete flow at this radial position goes in a backward direction against the main flow direction. This is a result of the blockage of the blade passage by the lifted hub vortex and the tip leakage flow that also has a reversed flow direction.
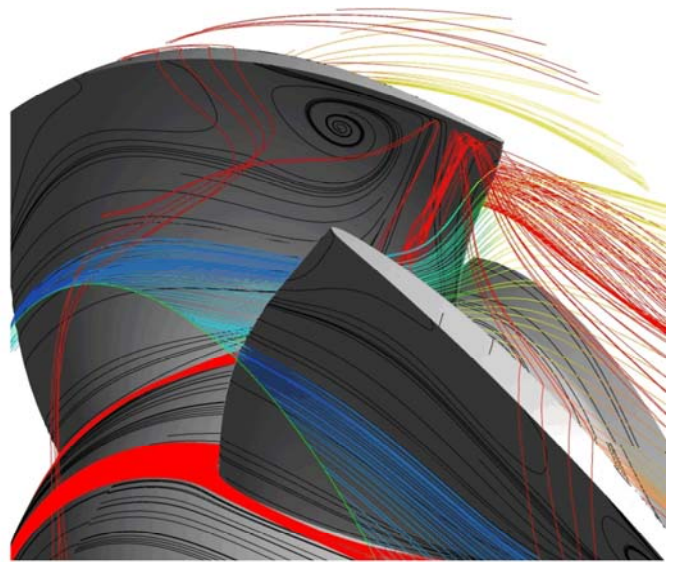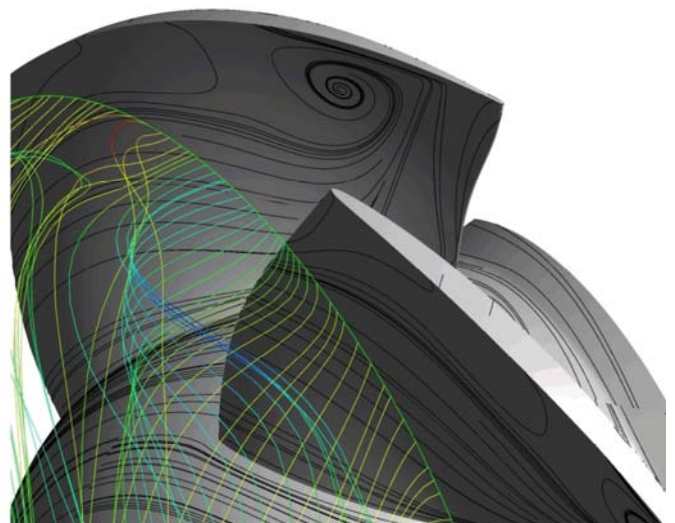

R/R$_{Shroud}$=0,71
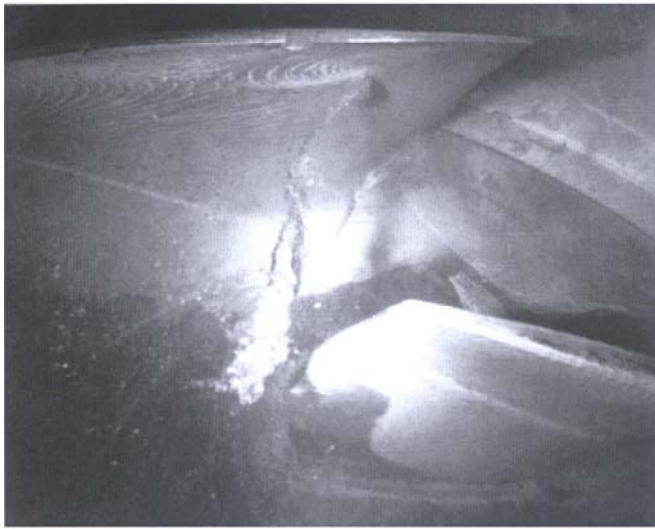
R/R$_{Shroud}$=0,81
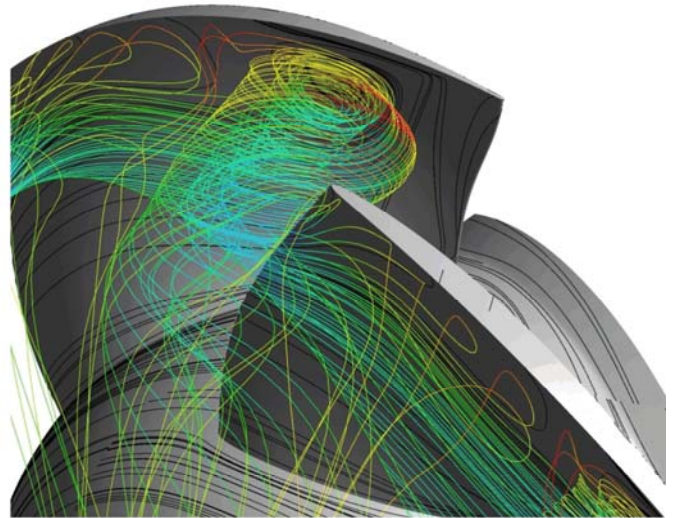
FLOW STRUCTURE AT BLADE TIP

In the last part of the discussion the flow field in the blade tip region is of interest. The left side of figure 15 represents in a photograph obtained by Golz [1] the core region of the cavitating vortex core of the tip clearance vortex for different operating points. At the right side the representation of the tip clearance vortex from the numerical results is shown by streamlines starting in the tip gap and a vortex core region. The hub and blade wall is colored with the static pressure.

In the upper picture in figure 15 for Q/Q_{Bep}=1.4 the leakage flow in the first third of the chord length of the blade has a direction from suction to pressure side. Up to this chord length

R/R$_{Shroud}$=0,95

Figure 14: Wall streamlines at blade pressure side and streamlines at different radial positions Q/Q_{Bep}=0.32.

the direction of the tip leakage flow is changed to the direction from pressure to suction side and the tip clearance vortex is formed. The position of the vortex core region in the computation compared with that of the photograph is satisfactory.

At $Q/Q_{Bep}=0.96$, represented in the middle picture of figure 15, the flow conditions in the tip gap are changed in such a way that the leakage flow starts directly at the blade leading edge with a direction from pressure to suction side. Consequently, the starting-point of the vortex core region in the calculation is moved upstream and starts now at the blade leading edge. The angle between vortex core and the stagger angle of the blade is increased and the vortex core travels further into the blade passage, as can be seen by comparing the black streamlines in the right parts at the middle and upper picture of figure 15. The photograph by Golz at the left side in the middle shows the same characteristics.

The lower picture in figure 15 compares the situation close to the beginning of stall at the stable part of the pump characteristic at $Q/Q_{Bep}=0.69$ in the computation on the right and $Q/Q_{Bep}=0.74$ in the photographed operating point on the left. In this operating range a spiral type vortex breakdown of the tip clearance vortex of this pump was detected and described by Schrapp [3] and also by Golz [1]. In the left figure the cavitating vortex core loses its straight shape. From this angle it seems that the vortex core moves forward and backward in an axial direction. The representation of the numerical results at the right side also shows a tendency to the same behavior.

This numerical result has to be explained in more detail. To this end the characteristic shown in figure 16 is used. In this figure the measured results [1] used in figure 6 are printed. The points represent the results of a computation that starts close to the beginning of stall in stable operation conditions. In this transient calculation the resistance coefficient of flow resistance 2 described in figure 3 is continuously increased during the calculation. This has an equivalent effect to closing the throttle valve behind the pump during operation. Therefore the points representing the calculated results show the transient change of the pump head and mass flow during the transition from stable operation to nearly stall conditions. This explains the difference between computation and measurement representing different stable stationary operating points and not the transient change. The numerical effort required for this computation was huge, so each point plotted in figure 16 represents the average of head and mass flow during one impeller revolution. This means more than 60 revolutions are computed. For this computation the time step was reduced so that a rotation of the impeller of one degree was represented in each time step to get a very good convergence with max. RMS values below $9x10^{-4}$ in every point for each equation. This type of computation is only possible with the new numerical model without constant inlet and outlet boundary conditions that we have introduced here. These results could be used for comparison with transient measurements.

To make the flow structure of the tip leakage vortex in this operation range clearer, figure 17 is used. In the upper part of this figure is a photograph taken by Golz [1] of the cavitating tip leakage vortex at 80% design mass flow rate. The direction of view is from the blade trailing edge upstream towards the blade leading edge. The leading edge itself is hidden by a part of the casing. In the lower part the calculated result at 69% design mass flow rate during the transient calculation is presented from the same perspective. The blade surface is coloured with the static pressure and the distribution of the static pressure is shown in white lines at the shroud wall. Inside the tip gap streamlines are generated by integrating in forward direction only. These are in black and additionally a vortex core region with a constant grey color is generated. It is therefore apparent that the vortex core in the computation also obtains a three-dimensional spiral shape, as can be seen in the photograph. This indicates that this computation is also able to reproduce the spiral type vortex breakdown that was found experimentally in this pump. As far as the authors know this is the first time that such a vortex breakdown in a turbomachine has been obtained by experimental and numerical methods in the same machine at almost the same operating point.

CONCLUSIONS

In this paper a new numerical model is presented to calculate the flow field, especially at unstable operating points. This is done by simulating an axial flow pump. The results obtained by this simulation method are compared with the experimental results of Golz [1,2], Schrapp [3] and Kosyna [4]. A comparison with earlier numerical results described in [5-8] is also made. The differences found for operation points in the stable range as well as in the deep stall region are marginal only. During the comparison with earlier results for different operating points the changes in the structure and also some details of the flow field are described. We also demonstrate the ability to simulate the transition from stable operation to stall as a transient process by changing only the resistance coefficient in the part of the set-up representing the valve. This allows us to investigate the unstable flow structures in detail by numerical simulations. In the sample computation carried out to demonstrate this ability the spiral type vortex breakdown already found in experimental investigations by Golz [1] and Schrapp [3] was also found in the numerical results. To the authors' knowledge this is the first time that this type of vortex breakdown has been found in the same turbomachine experimentally and by numerical investigations.
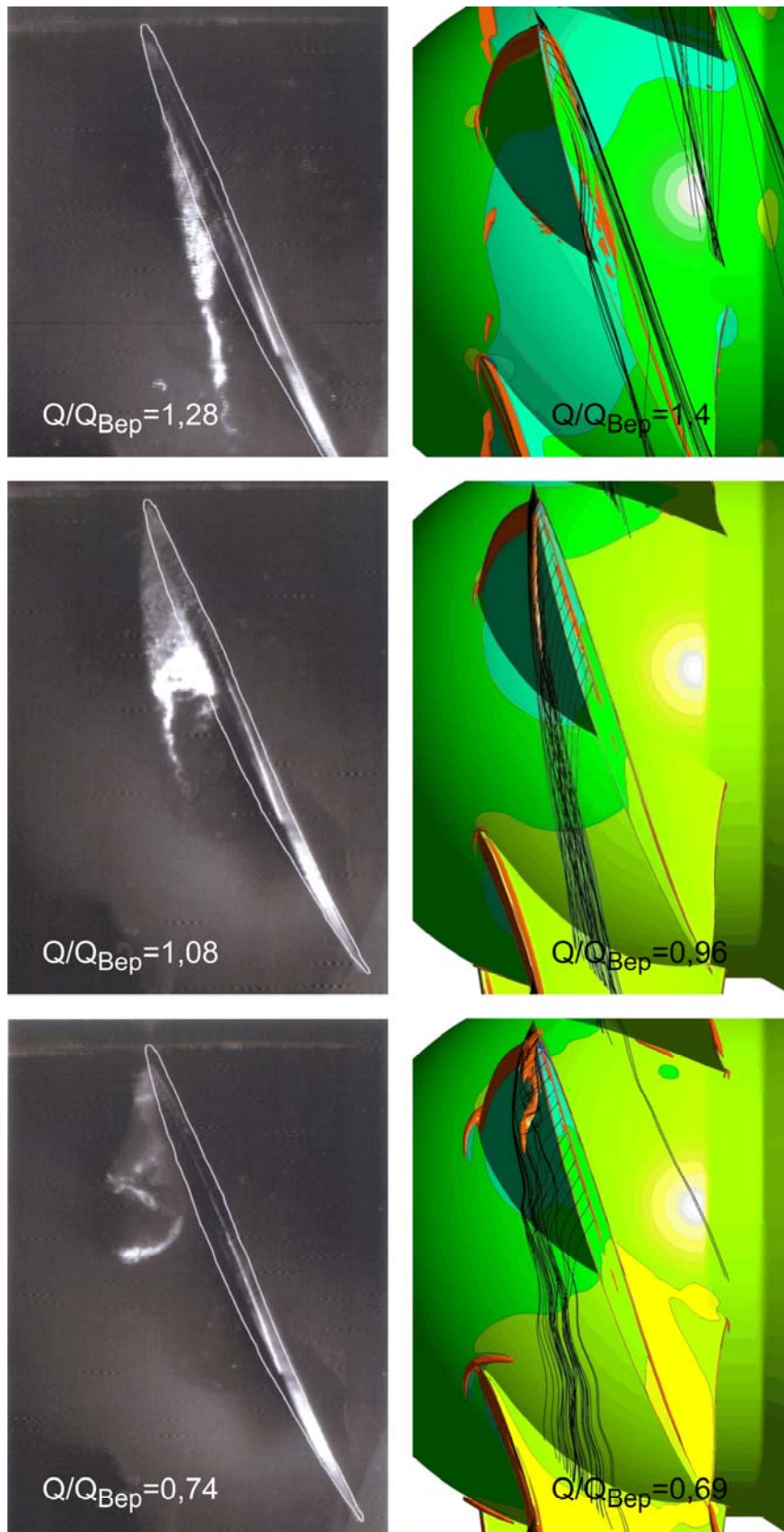
Figure 15: Cavitating tip leakage vortex (photograph taken by Golz [1]) at left side and streamlines in tip gap with vortex core region from computation at right side for different operating points.
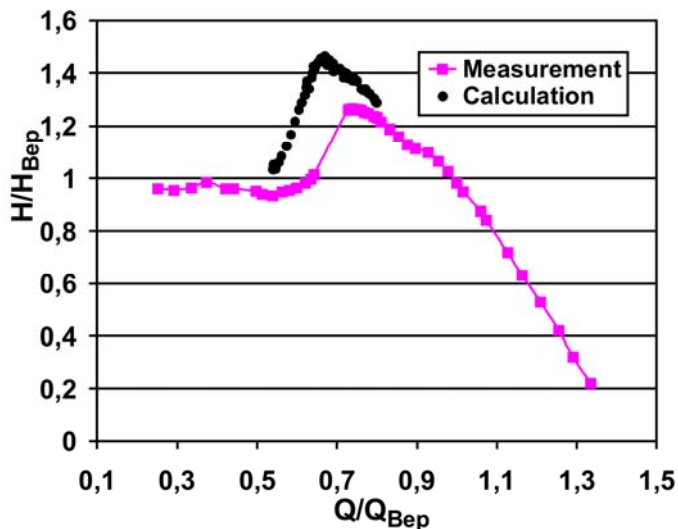
Figure 16: Pump head characteristic transient calculation, measured by Golz [1].

REFERENCES

[1] Goltz, I., 2006, „Entstehung und Unterdrückung der Kennlinieninstabilität einer Axialpumpe", Mitteilungen des Pfleiderer-Instituts für Strömungsmaschinen, Heft 10, März 2006

[2] Goltz, I., Kosyna, G., Wulff, D., Schrapp, H., Stark, U1., Saathoff, H., Bross, S., 2004, „Structure of the Rotor Tip Flow in a Highly Loaded Single-Stage Axial-Flow Pump Approaching Stall, Part II: Stall Inspection – Understanding the Mechanism and Overcoming its Negative Impacts", Proceedings of ASME Heat Transfer/Fluids Engineering Summer Conference, HT-FED04, Charlotte, North Carolina, USA

[3] Schrapp, H., Stark, U., Goltz, I., Kosyna, G., Bross, S., 2004, „Structure of the Rotor Tip Flow in a Highly Loaded Single-Stage Axial-Flow Pump Approaching Stall, Part I: Breakdown of the Tip-Clearence Vortex", Proceedings of ASME Heat Transfer/Fluids Engineering Summer Conference, HT-FED04, Charlotte, North Carolina, USA

[4] Kosyna, G., Goltz, I., Stark, U., 2005, „Flow Structure of an Axial Flow Pump from Stable Operation to Deep Stall", Proceedings of ASME Fluids Engineering Summer Conference, FEDSM 2005, Houston, Texas, USA

[5] Benra, F. - K., Dohmen, H. J., Schmidt, M., 2007, „Flow Phenomena in a Highly-Loaded Single-Stage Axial-Flow Pump Comparison of Experimental and Numerical Results", FEDSM 2007, San Diego, California, USA

[6] Benra, F. - K., Dohmen, H. J., 2008, „Unsteady Three-Dimensional Flow Phenomena in an Axial Flow Pump at Different Operating Points", FEDSM 2008, Jacksonville, Florida, USA

[7] Benra, F. - K., Dohmen, H. J., 2008, „Part Load Characteristic Investigation of a Highly Loaded Axial Flow Pump with Casing Treatment Comparison of
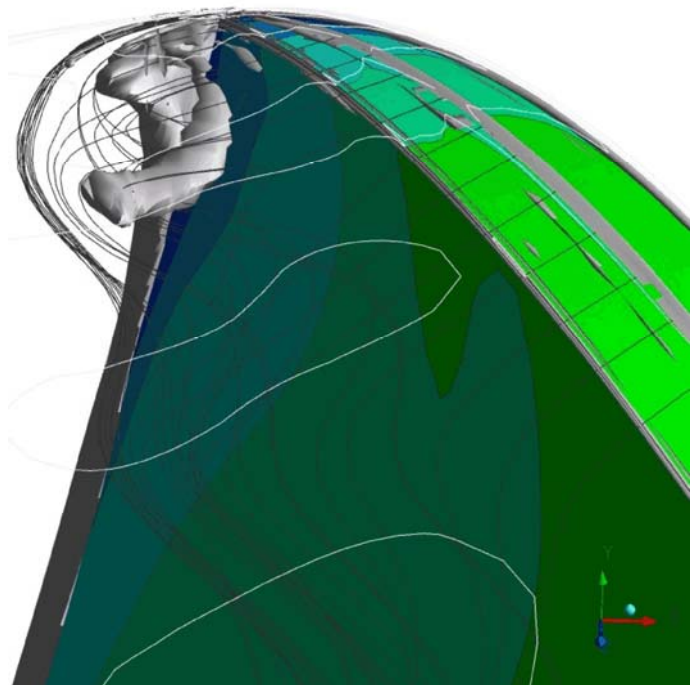
Figure 17: 3-D structure of tip clearance vortex at breakdown conditions (photograph taken by Golz [1]) Q/QBep=0,.8 upper, calculation Q/QBep=0.69 lower.

Experimental and Numerical Results", IAHR 2008, Foz do Iguassu, Brazil

[8] Pérez Flores, P., Kosyna, G., Benra, F. - K., Dohmen, H. J., Gandhi, B. K., Kumar, M., 2009, „ Improvement of Axial-Flow Pump Part Load Behaviour – an experimental and numerical Study", CMFF09, Budapest, Hungary